Unsteady Viscous-Inviscid Interaction Procedures for Transonic Airfoils Using Cartesian Grids

Charles C. Fenno Jr.*
North Carolina State University, Raleigh, North Carolina
Perry A. Newman†
NASA Langley Research Center, Hampton, Virginia
and
H. A. Hassan‡
North Carolina State University, Raleigh, North Carolina

A viscous-inviscid interaction procedure for transonic airfoils using an Euler/integral boundary-layer formulation and Cartesian grids is presented. The approach is based on a time-dependent formulation for both the integral boundary-layer equations and the Euler equations. Effects of upstream history on the shear stress are modeled by a time-dependent rate equation derived from the turbulent kinetic energy equation. The importance of the various terms in this equation are discussed in detail. Results are presented for two of the test cases reported for the RAE 2822 supercritical airfoil, and one of the cases reported for the NACA 0012 symmetric airfoil. In addition, these results are compared to solutions of the Navier-Stokes equations using a variety of turbulence models. In general, good agreement is indicated.

Introduction

THIS research is part of an ongoing effort designed to use Cartesian grids in the solution of the Euler and Navier-Stokes equations. Cartesian grids are simple to construct and may therefore result in more efficient computational schemes when complex shapes are considered. When used in conjunction with typical aircraft shapes, they result in a variety of polygonal and triangular surface cells with randomly distributed volumes (Fig. 1). Calculations using such grids were successfully demonstrated for the Euler equations in two and three dimensions.[1,2] However, it became evident recently[3] that Cartesian grids with randomly distributed surface cell areas are not suited for the Navier-Stokes equations. Therefore, one purpose of this work is to show that such grids can still be used for the calculation of attached and separated turbulent flows using an Euler/integral turbulent boundary-layer formulation.

An eventual objective of this approach is to extend it to three-dimensional geometries. Because the marching direction in three-dimensional boundary-layer calculations is not well defined, a time-dependent boundary-layer approach is used.[4] Thus, a time-dependent boundary-layer formulation similar to that used by Donegan[5] is implemented.

The various turbulent correlations employed were developed by Whitfield et al.[6] and later updated and improved by Thomas.[7,8] Both equilibrium and nonequilibrium turbulence are considered. In order to account for departure from equilibrium, a time-dependent rate equation for the shear stress is derived from the kinetic energy equation. The derivation follows the procedure used by Green et al.[9] and Thomas.[8] The equation used by Thomas does not take into consideration the effects of diffusion and advection normal to the boundary layer. A recent turbulence model by Johnson and King[10] demonstrated the importance of the diffusion term in predicting the shock wave location in separated transonic flows. Because of this, an additional objective of this work is to study the effects of including/excluding advection and diffusion terms in the turbulent kinetic energy equation.

Most viscous-inviscid iteration procedures assume the wake to lie along $y = 0$, or the trailing-edge grid line, when body-fitted grids are employed. The importance of utilizing the correct wake shape was emphasized by Le Balleur.[11] Because of this, the present work also incorporates an approximate procedure for locating the position of the wake cut.

Formulation of the Problem

Integral Boundary-Layer Equations

The integral boundary-layer formulation is based on the mean flow kinetic energy, or dissipation integral method. The formulation was developed originally by Whitfield et al.[6] and updated by Thomas.[7,8] This approach was found to yield results that are quite similar to the entrainment integral method.[8] The time-dependent momentum integral equation can be written as[5]

$$\frac{1}{\rho_e u_e^2}\left[\frac{\partial}{\partial t}(\rho_e u_e \delta^*) - u_e \frac{\partial}{\partial t}(\rho_e \theta_\rho)\right] + \frac{1}{\rho_e u_e^2}\frac{\partial}{\partial s}(\rho_e u_e^2 \theta) + \frac{\delta^*}{u_e}\frac{\partial u_e}{\partial s} = \frac{c_f}{2} \tag{1}$$

where s is the distance along the wall, ρ is the density, u is the velocity, and subscript e denotes conditions at the edge of the viscous boundary layer. The displacement thickness δ^*, momentum thickness θ, and density thickness θ_ρ appearing in Eq. (1) are defined as

$$\delta^* = \int_0^\infty \left(1 - \frac{\rho u}{\rho_e u_e}\right) dy \tag{2a}$$

$$\theta = \int_0^\infty \frac{\rho u}{\rho_e u_e}\left(1 - \frac{u}{u_e}\right) dy \tag{2b}$$

Received April 9, 1988; presented as Paper 88-2591 at the AIAA 6th Applied Aerodynamics Conference, Williamsburg, VA, June 6-8, 1988; revision received Feb. 22, 1989.

*Research Assistant, Mechanical and Aerospace Engineering. Student Member AIAA.
†Senior Research Scientist, Theoretical Aerodynamics Branch, Transonic Aerodynamics Division.
‡Professor, Mechanical and Aerospace Engineering. Associate Fellow AIAA.

$$\theta_\rho = \int_0^\infty \left(1 - \frac{\rho}{\rho_e}\right) dy \tag{2c}$$

The skin-friction coefficient c_f is the shear stress at the wall τ_w normalized by the edge dynamic pressure

$$\frac{c_f}{2} = \frac{\tau_w}{\rho_e u_e^2} \tag{3}$$

The second equation is obtained by multiplying the streamwise momentum equation by the streamwise velocity and integrating normal to the wall. The resulting equation can be written as

$$\frac{1}{2\rho_e u_e^3}\frac{\partial}{\partial t}[\rho_e u_e^2(\theta + \delta^* - \theta_\rho)] + \frac{\theta_\rho - \delta^* + \delta^{**}}{u_e^2}\frac{\partial u_e}{\partial s}$$
$$+ \frac{1}{2\rho_e u_e^3}\frac{\partial}{\partial s}(\rho_e u_e^3 \theta^*) + \frac{\delta^{**}}{u_e}\frac{\partial u_e}{\partial s} = D \tag{4}$$

The compressibility thickness δ^{**}, energy thickness θ^*, and dissipation integral D appearing in Eq. (4) are defined as

$$\delta^{**} = \int_0^\infty \frac{u}{u_e}\left(1 - \frac{\rho}{\rho_e}\right) dy \tag{5a}$$

$$\theta^* = \int_0^\infty \frac{\rho u}{\rho_e u_e}\left(1 - \frac{u^2}{u_e^2}\right) dy \tag{5b}$$

$$D = \frac{1}{\rho_e u_e^2}\int_0^\infty \tau \frac{\partial}{\partial y}\left(\frac{u}{u_e}\right) dy \tag{5c}$$

where τ represents the total shear stress. In the derivation of Eqs. (1) and (4), the velocity vector at the wall is taken to be zero.

The governing equations contain nine unknowns. A closure procedure is employed that expresses six of the unknowns in terms of the remaining three, which are the displacement and momentum thicknesses and the edge Mach number. An inverse procedure is employed with δ^* being specified and updated using a procedure developed by Carter.[12] The closure relations used are those developed by Thomas and are appropriate for both attached and separated flows. The relations are summarized in the Appendix.

Dissipation Integral

The dissipation integral is one of the most important terms in the integral boundary-layer equations because its evaluation is dependent on the turbulence model employed. For equilibrium boundary layers, the dissipation integral is determined as the sum of contributions from inner and outer regions of the boundary layer. Thus, in the inner region the total shearing stress is assumed constant, while in the outer region Clauser's eddy viscosity model,[13] i.e.,

$$\tau_o = \rho\epsilon\frac{\partial u}{\partial y}, \qquad \epsilon = 0.0168 u_e \delta^* \tag{6}$$

is employed. Thus,

$$D = D_i + D_o$$

with

$$D_i = \left|\frac{\bar{c}_f}{2}\right|^{3/2}\frac{\pi}{0.018} \tag{7a}$$

$$D_o = \bar{D}_o(1 + 0.025\, M_e^{1.4})^{-1} \tag{7b}$$

$$\bar{D}_o = 0.0168\left(\frac{2}{3}\frac{\bar{H} - 1}{\bar{H}}\right)^3\frac{\pi^2}{2} \tag{7c}$$

where $\bar{H}$ is the displacement-thickness shape factor with the bar indicating an incompressible property.

Calculation of nonequilibrium boundary layers requires the use of a rate equation, which allows for a shear stress history. The rate equation is usually based on the turbulent kinetic energy equation. Using assumptions introduced by Bradshaw et al.,[14] Green et al.[9] reduced the turbulent kinetic energy to an equation for the maximum shear stress. Using a similar procedure, an equation that contains the time-dependent terms can be written as

$$\frac{\delta}{uC_\tau}\frac{\partial C_\tau}{\partial t} + \frac{\delta}{C_\tau}\frac{\partial C_\tau}{\partial s} = 2a_1\frac{u_e}{u}\frac{\delta}{L}(C_{\tau_{EQ}}^{1/2} - C_\tau^{1/2})$$
$$+ \left(\frac{2\delta}{u_e}\frac{\partial u_e}{\partial s}\right)_{EQ} - \frac{2\delta}{u_e}\frac{\partial u_e}{\partial s} \tag{8}$$

where

$$C_\tau = \frac{\tau_{max}}{\rho u_e^2} \tag{9}$$

Bradshaw et al.[14] defined a_1 to be a constant equal to 0.15. Thomas related C_τ to the outer contribution of the dissipation integral

$$C_\tau = 0.295\,\bar{D}_o^{5/3} \tag{10}$$

As a result, the equation governing $\bar{D}_o$ follows from Eqs. (8) and (10) as

$$\frac{\delta^*}{u_e}\frac{u}{u_e}\frac{1}{\bar{D}_o}\frac{\partial \bar{D}_o}{\partial t} + \frac{\delta^*}{\bar{D}_o}\frac{\partial \bar{D}_o}{\partial s} = 0.244\frac{u_e}{u}\frac{\delta}{L}\frac{\delta^*}{\delta}(\bar{D}_{oEQ}^{1/3} - \bar{D}_o^{1/3})$$
$$+ 3\frac{\delta^*}{\delta}\left(\frac{\delta}{u_e}\frac{\partial u_e}{\partial s}\right)_{EQ} - \frac{3\delta^*}{u_e}\frac{\partial u_e}{\partial s} \tag{11}$$

Thomas evaluated the first term on the right-hand side of Eq. (11) as

$$\frac{\delta^*}{\delta}\lambda(\bar{D}_{oEQ}^{1/3} - \bar{D}_o^{1/3})$$

with

$$\frac{\delta^*}{\delta} = \frac{2}{3}\left(\frac{\bar{H} - 1}{\bar{H}}\right), \qquad \lambda = 5.0\left[1 + \left(\frac{\bar{H} - 1}{\bar{H}}\right)^3\right] \tag{12}$$

Green et al. assumed u_e/u to be a constant equal to 1.5, but Thomas[8] provided the relationship

$$\frac{u_e}{u} = \frac{3\bar{H}}{\bar{H} + 2} \tag{13}$$

Thus, the desired rate equation takes the form

$$\frac{\delta^*}{u_e\bar{D}_o}\left(\frac{3\bar{H}}{\bar{H} + 2}\right)\frac{\partial \bar{D}_o}{\partial t} + \frac{\delta^*}{\bar{D}_o}\frac{\partial \bar{D}_o}{\partial s} = \frac{10}{3}\left(\frac{\bar{H} - 1}{\bar{H}}\right)\left[1 + \left(\frac{\bar{H} - 1}{\bar{H}}\right)^3\right]$$
$$\times (\bar{D}_{oEQ}^{1/3} - \bar{D}_o^{1/3}) + \left(\frac{2\delta}{u_e}\frac{\partial u_e}{\partial s}\right)_{EQ} - \frac{3\delta^*}{u_e}\frac{\partial u_e}{\partial s} \tag{14}$$

Thomas retained only the first term on the right-hand side of Eq. (14), which represents the difference between production and dissipation effects. The present work investigates the inclusion of the second term, which represents effects due to diffusion, and the third term, which represents effects due to advection normal to the boundary layer. Green et al. defined the diffusion term as

$$\left(\frac{2\delta}{u_e}\frac{\partial u_e}{\partial s}\right)_{EQ} = \frac{2.5(H_{\delta^*} + H_1)}{H_{\delta^*}}\left[\frac{c_f}{2} - \left(\frac{\bar{H} - 1}{6.432\bar{H}}\right)^2\frac{1}{1 + 0.04M_e^2}\right] \tag{15}$$

where

$$H_1 = 3.15 + \frac{1.72}{H_{\delta^*} - 1} - 0.01(H_{\delta^*} - 1)^2 \tag{16}$$

Euler Equations

The integral form of the Euler equations in Cartesian coordinates can be written for a region Ω, with boundary $\partial\Omega$, as

$$\frac{\partial}{\partial t}\iint_\Omega W\,dx\,dy + \int_{\partial\Omega}(F\,dy - G\,dx) = 0 \tag{17}$$

where

$$W = \begin{bmatrix} \rho \\ \rho u \\ \rho v \\ \rho E \end{bmatrix} \quad F = \begin{bmatrix} \rho u \\ \rho u^2 + p \\ \rho uv \\ \rho uH \end{bmatrix} \quad G = \begin{bmatrix} \rho v \\ \rho vu \\ \rho v^2 + p \\ \rho vH \end{bmatrix}$$

and, for a perfect gas,

$$E = \frac{p}{(\gamma - 1)\rho} + \frac{1}{2}(u^2 + v^2) \tag{18a}$$

$$H = E + p/\rho \tag{18b}$$

In these equations, ρ is the density, u and v are the velocity components in the x and y directions, p is the pressure, and E and H are the total energy and enthalpy, respectively.

The method of discretization and solution are detailed in Ref. 1. In particular, the computational domain is divided into a number of quadrilateral cells and Eq. (17) is applied to each cell. This leads to an ordinary differential equation for each cell of the form

$$\frac{\mathrm{d}}{\mathrm{d}t}(hW) + Q(W) = 0 \tag{19}$$

where h represents the cell area and the Q operator represents the second term in Eq. (17). A cell-centered scheme is employed; thus, quantities at cell faces are taken as averages of quantities at adjoining cell centers. For equal cells, such a scheme is equivalent to a central-difference scheme.

Interaction Procedure

The viscous-inviscid interaction method involves the solution of two separate sets of equations, the integral boundary-layer equations, and the Euler equations. The integral boundary-layer equations and the correlations required for closure result, when equilibrium turbulence is considered, in a system of two equations for the two dependent variables M_e and $\bar{H}$. A third variable δ^* is calculated by iteration according to the relation[12]

$$\delta^{*n+1} = \delta^{*n}\left[1 + \omega\left(\frac{u_{e,v}}{u_{e,i}} - 1\right)\right] \tag{20}$$

where ω is a relaxation factor (about 0.25) and $u_{e,v}$ and $u_{e,i}$ are the edge velocities calculated from the viscous and inviscid equations, respectively. The link between the viscous and inviscid equations is provided by the interface, or edge boundary condition. The most straightforward procedure is to displace the wall a distance equal to δ^* and apply appropriate conditions there. This requires, however, that a new grid be generated each time δ^* changes. It has been shown by Lighthill[15] that the influence of the viscous boundary layer on the inviscid flow can be accounted for by applying a transpiration boundary condition at the wall. Such a boundary condition can be derived from the conservation of mass equation and can be expressed as

$$\rho_e V_n = \frac{\partial}{\partial s}(\rho_e u_e \delta^*) \tag{21}$$

where subscript n designates conditions normal to the wall. For adiabatic wall conditions, Eq. (21) is the only edge condition needed.

The nonzero mass flux at the wall resulting from Eq. (21) is incorporated into the Euler equations through flux summation at the wall by requiring the velocity components there to be (see Fig. 2)

$$u_w = u_{e,v}\cos\beta - V_n \sin\beta \tag{22a}$$

$$v_w = u_{e,v}\sin\beta + V_n \cos\beta \tag{22b}$$

Wake Location

The location of the wake cut is determined by the location of the streamline leaving the trailing edge of the airfoil. The integral boundary-layer equations are integrated beyond the airfoil along the wake cut for a distance of one-half of a chord length. The skin friction that appears in the equations is set to zero in this wake region. The transpiration velocity is calculated as before. However, it is not imposed on the cut but on the cell surfaces as shown in Fig. 3. This makes it possible to

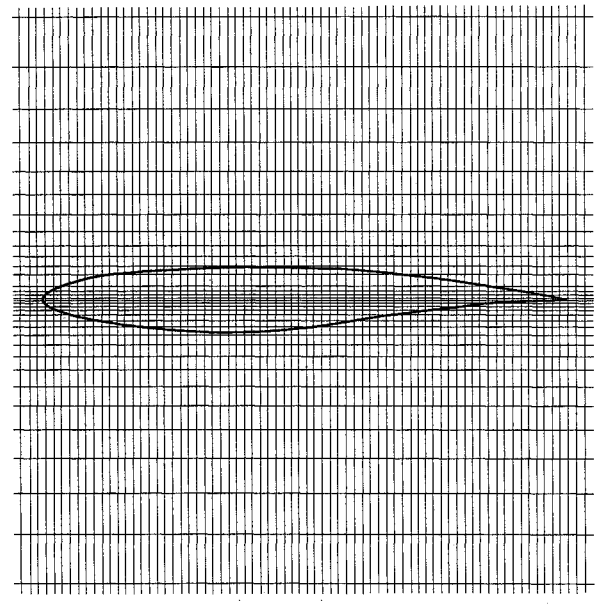

Fig. 1 Typical Cartesian grid over an airfoil.

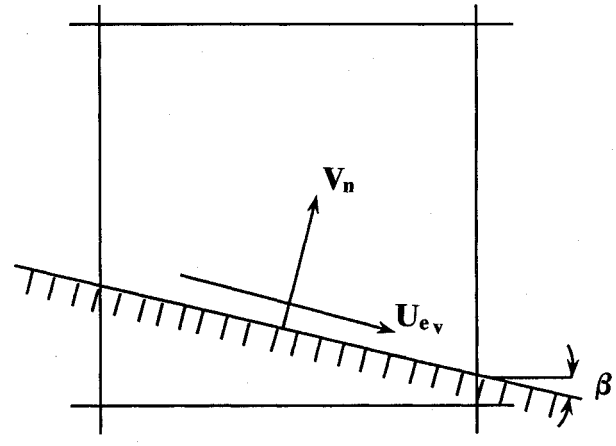

Fig. 2 Cartesian cell intersection with body.

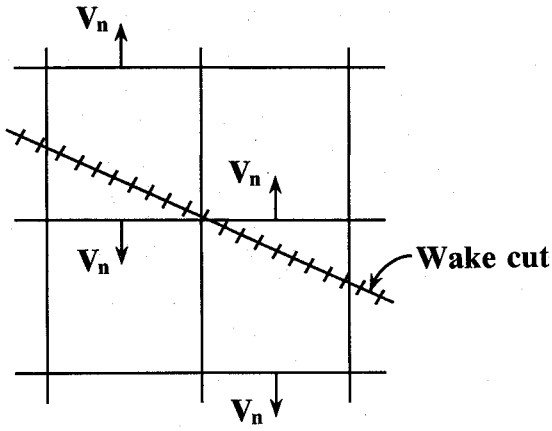

Fig. 3 Wake cut following a streamline.

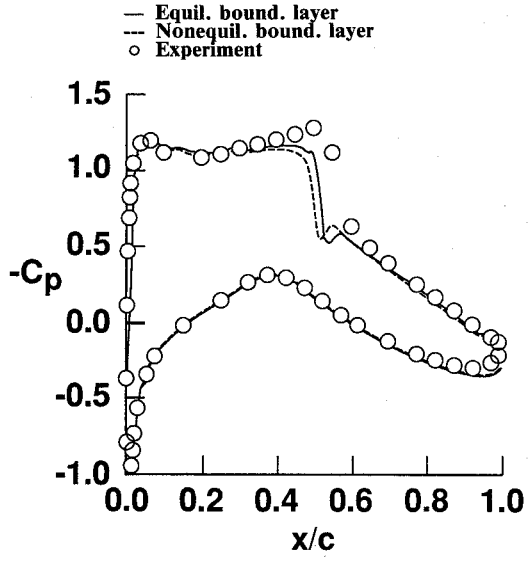

Fig. 4 Pressure coefficient vs x/c for the RAE 2822 airfoil at $M_\infty = 0.730$, $\alpha = 2.78$ deg, $Re_\infty = 6.5 \times 10^6$.

use the original grid. This procedure then greatly reduces the computational work while still providing for a good approximation to the position of the wake cut.

Time-Stepping Scheme

Both the Euler and the integral boundary-layer equations were integrated using the four stage Runge-Kutta time-stepping scheme of Jameson et al.[16] Local time stepping was used throughout, while enthalpy damping and residual smoothing were used to accelerate the convergence of the Euler equations.

Implementation of Computational Scheme

Starting with a uniform flow, the Euler equations are integrated for a number of time steps (about 100) at a Courant number of 5. During this initial integration, the mass flux at the wall is assumed zero. At this stage, the inviscid-flow solution provides an initial distribution of M_e along the airfoil for the boundary-layer equations. The initial distribution of $\bar{H}$ and δ^* are those for a flat plate at $M = 0$, i.e., $\bar{H}$ and $d\delta^*/ds$ are constants. The values used here at $\bar{H} = 1.4$ and $d\delta^*/ds = 6 \times 10^{-3}$. The location of the wake is also determined as the streamline leaving the trailing edge.

The interaction proceeds by integration of the boundary-layer equations until the value of the boundary-layer residual is less than that for the Euler equations. The distributions of δ^* and the transpiration velocity V_n are then calculated based on the latest available information. Next, the Euler equations

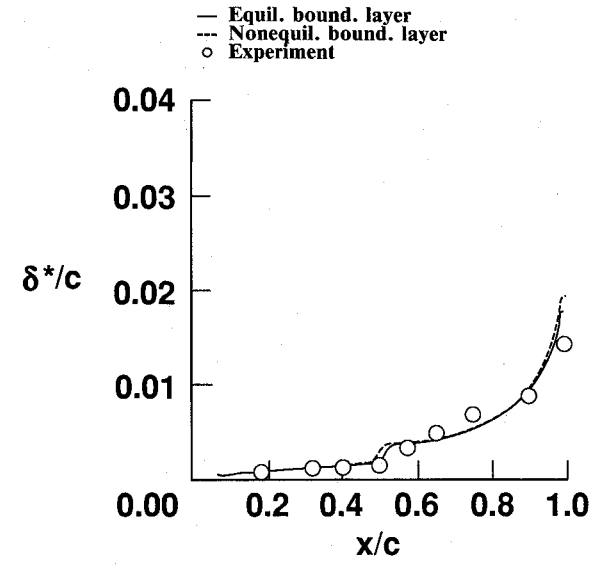

Fig. 5 Displacement thickness vs x/c for the RAE 2822 airfoil at $M_\infty = 0.730$, $\alpha = 2.78$ deg, $Re_\infty = 6.5 \times 10^6$.

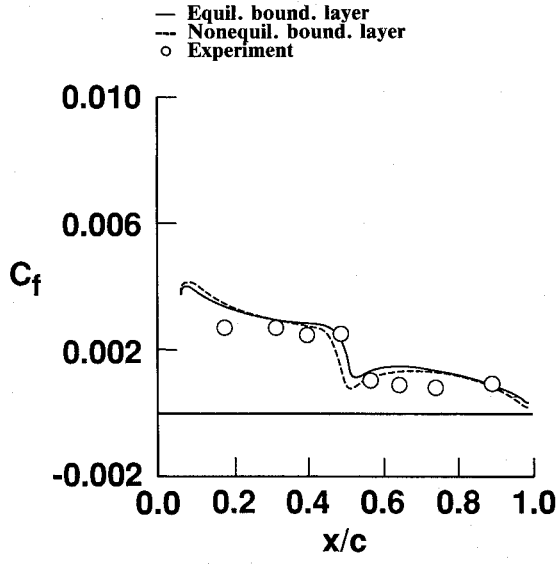

Fig. 6 Skin friction vs x/c for the RAE 2822 airfoil at $M_\infty = 0.730$, $\alpha = 2.78$ deg, $Re_\infty = 6.5 \times 10^6$.

are integrated a number of steps (about 10) using the new transpiration velocity and the process is repeated.

The edge velocities $u_{e,i}$ and $u_{e,v}$ are available from the solutions of the Euler and the integral boundary-layer equations, respectively. The ratio of edge velocities is a measure of the convergence of the interaction procedure. This ratio approaches unity as the equation sets arrive at a compatible solution. Interaction continues until $[(u_{e,v})/(u_{e,i}) - 1]$ is less than 10^{-2}–10^{-3}.

Results and Discussion

Results are presented for the RAE 2822 supercritical airfoil and for the NACA 0012 symmetric airfoil at various transonic flight conditions. Comparisons are made between the numerical results of the present work, the experimental data,[17,18] and solutions of the Navier–Stokes equations using various turbulence models.[19]

The first case considered is the RAE 2822 airfoil at $M_\infty = 0.73$, $\alpha = 2.78$ deg, and $Re_\infty = 6.5 \times 10^6$, corresponding to case 9 of Ref. 17. The angles of attack mentioned in this work include the free-air corrections suggested in the aforementioned references. The boundary layer was started at $x/c = 0.03$, corresponding to the transition trip location re-

ported in Ref. 17. The pressure-coefficient distribution for this attached flow case is shown in Fig. 4 for calculations in which equilibrium and nonequilibrium boundary layers are considered. The rate equation used in the nonequilibrium boundary-layer calculation included all of the terms on the right-hand side of Eq. (14). As is seen in Fig. 4, nonequilibrium effects result in additional forward motion of the shock. Figures 5 and 6 show the boundary-layer displacement thickness and skin friction for the nonequilibrium boundary layers and compare these results with the experimental data. The displacement-thickness distribution shows the thickening of the boundary layer resulting from its interaction with the shock, which, in turn, is responsible for the forward movement of the shock. The skin-friction plot of Fig. 6 shows the expected drop in skin friction at the shock, with the drop being greater when nonequilibrium effects are taken into consideration. It should be noted that much of the oscillatory behavior observed in the present results, particularly in the pressure distributions, is a direct result of the random variation of the body surface cell volumes inherent in the Cartesian grid structure. This random cell-volume variation yields unsatisfactory solutions when the Navier-Stokes equations are employed,[3] but only causes slight oscillations in the present viscous-inviscid interaction procedure.

The second case presented is the RAE 2822 airfoil at $M_\infty = 0.75$, $\alpha = 2.81$ deg, and $Re_\infty = 6.2 \times 10^6$, which is case 10 of Ref. 17. This case involves flow separations at the foot of the shock wave. Figure 7 shows the pressure-coefficient distributions for equilibrium and nonequilibrium boundary-layer calculations. As with the previous case, the full rate equation is used for the nonequilibrium calculations. When nonequilibrium effects are considered, less pressure overshoot at the shock is indicated. Figure 8 shows that the displacement thickness is better predicted by the nonequilibrium boundary layer. The skin friction shown in Fig. 9 indicates that separation is predicted only when nonequilibrium effects are considered.

The next case considered is the NACA 0012 airfoil at $M_\infty = 0.799$, $\alpha = 2.26$ deg, and $Re_\infty = 9 \times 10^6$, and is compared to the experimental data reported by Harris.[18] The boundary layer for this case was started at $x/c = 0.05$, corresponding to the transition trip location reported in Ref. 18. The pressure-coefficient distribution is presented in Fig. 10. The most notable result is the pressure overshoot at the shock, which shows similar trends as for the RAE 2822 airfoil cases.

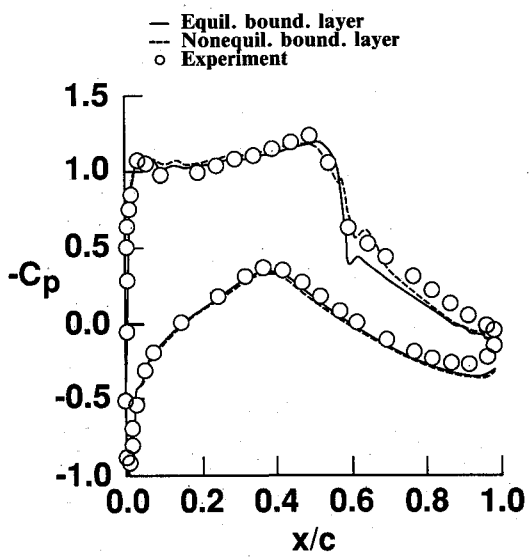

Fig. 7 Pressure coefficient vs x/c for the RAE 2822 airfoil at $M_\infty = 0.750$, $\alpha = 2.81$ deg, $Re_\infty = 6.2 \times 10^6$.

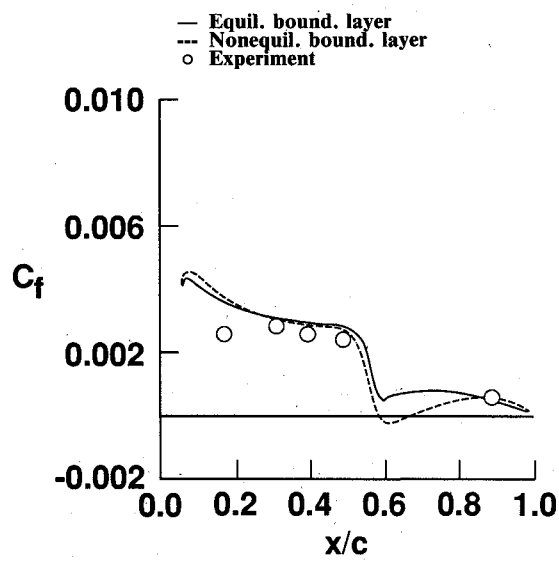

Fig. 9 Skin friction vs x/c for the RAE 2822 airfoil at $M_\infty = 0.750$, $\alpha = 2.81$ deg, $Re_\infty = 6.2 \times 10^6$.

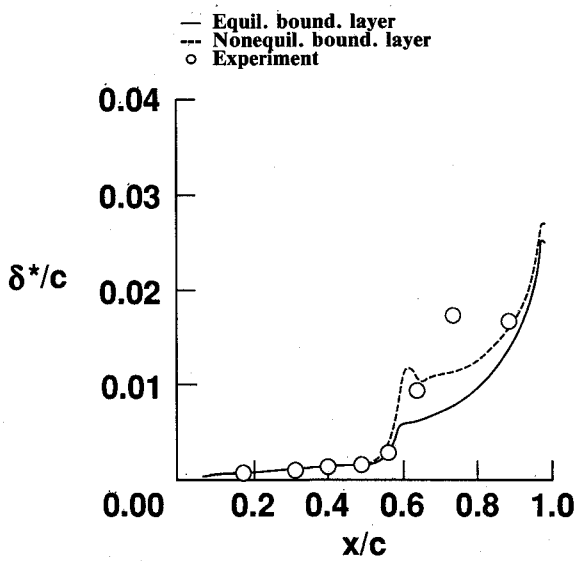

Fig. 8 Displacement thickness vs x/c for the RAE 2822 airfoil at $M_\infty = 0.750$, $\alpha = 2.81$ deg, $Re_\infty = 6.2 \times 10^6$.

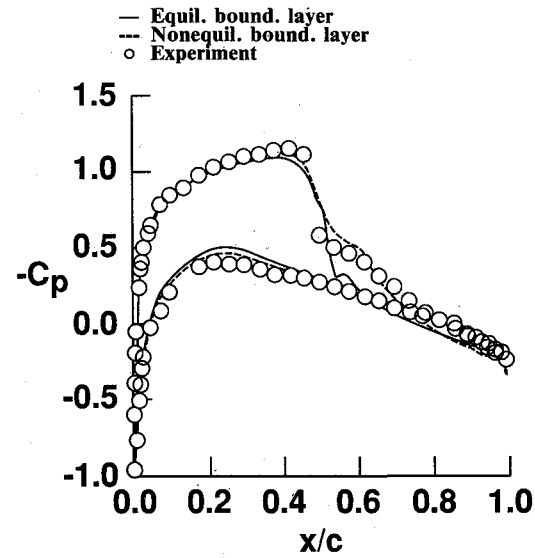

Fig. 10 Pressure coefficient vs x/c for the NACA 0012 airfoil at $M_\infty = 0.799$, $\alpha = 2.26$ deg, $Re_\infty = 6.2 \times 10^6$.

The cases described here show a significant difference between calculations involving equilibrium and nonequilibrium effects. This is more evident in the values of the lift and drag coefficients shown in Table 1. The equilibrium boundary-layer calculations predicted lift more accurately for the two RAE 2822 cases. These cases involve minimal separation effects and are well represented by an equilibrium formulation. The NACA 0012 case, with its large separation zone, shows a better lift-coefficient prediction for the nonequilibrium calculation using the full rate equation. The drag predictions were more varied than the lift predictions. For all cases, consideration of nonequilibrium effects resulted in the best drag prediction.

A comparative study was conducted into the effectiveness of the diffusion term and the normal advection term of the rate equation. Previous research neglected these terms.[7,8] Work by Johnson and King[10] indicated, however, that inclusion of the diffusion term improved the prediction of the shock location. Results are presented in Figs. 11–13 for calculations using the full rate equation, the rate equation without the normal advection term, and the rate equation without either diffusion or normal advection terms as used in Refs. 7 and 8. In all cases, the rate equation without normal advection showed higher pressures on the upper surface, lower pressures on the lower surface, and shock locations further forward as compared to both the full rate equation calculations and calculations involving the rate equation without diffusion or normal advection terms. Also, calculations using the rate equation without diffusion or normal advection terms resulted in pressures that were generally between the other two calculations. From this, it is evident that the diffusion term pushed the shock location forward and adjusted the pressure levels as mentioned, whereas the normal advection term tended to counteract the diffusion effects. This negation of diffusion by

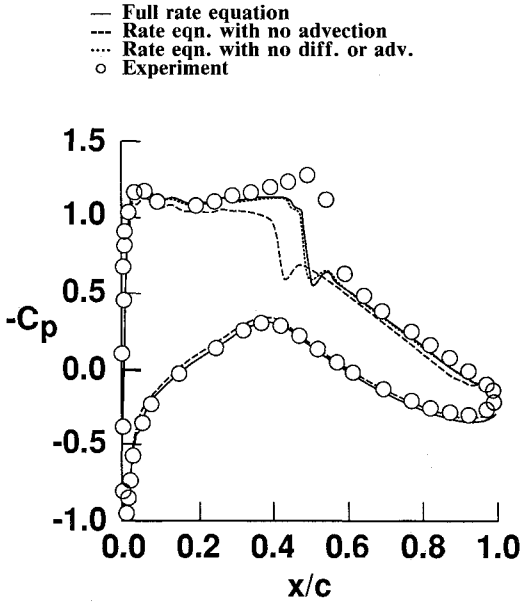

Fig. 11 Comparison of pressure coefficients for the various rate equations vs x/c for the RAE 2822 airfoil at $M_\infty = 0.730$, $\alpha = 2.78$ deg, $Re_\infty = 6.5 \times 10^6$.

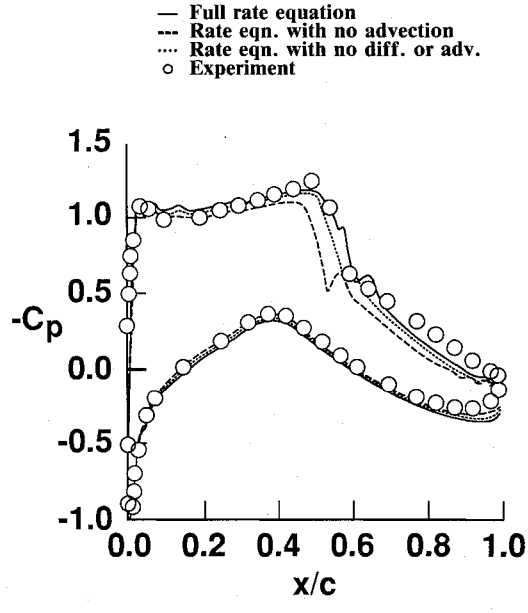

Fig. 12 Comparison of pressure coefficients for the various rate equations vs x/c for the RAE 2822 airfoil at $M_\infty = 0.750$, $\alpha = 2.81$ deg, $Re_\infty = 6.2 \times 10^6$.

Table 1 Lift and drag coefficients

	RAE 2822[a]		RAE 2822[b]		NACA 0012[c]	
	Value	% error	Value	% error	Value	% error
Lift coefficient C_l:						
Experimental	0.803	0.0	0.743	0.0	0.390	0.0
Equilibrium boundary layer	0.766	4.6	0.736	0.9	0.287	26.4
Nonequilibrium (full)	0.737	8.2	0.784	5.5	0.360	7.7
Without advection	0.629	21.7	0.645	13.2	0.220	43.6
Without advection or diffusion	0.724	9.8	0.728	2.0	0.302	22.6
Drag coefficient C_d:						
Experimental	0.0168	0.0	0.0242	0.0	0.0331	0.0
Equilibrium boundary layer	0.0207	23.2	0.0259	7.0	0.0282	14.8
Nonequilibrium (full)	0.0192	14.3	0.0300	24.0	0.0337	1.8
Without advection	0.0148	11.9	0.0200	17.4	0.0233	29.6
Without advection or diffusion	0.0185	10.1	0.0253	4.5	0.0292	11.8

[a] $M_\infty = 0.730$, $\alpha = 2.78$ deg, $Re_\infty = 6.5 \times 10^6$. [b] $M_\infty = 0.750$, $\alpha = 2.81$ deg, $Re_\infty = 6.2 \times 10^6$.
[c] $M_\infty = 0.799$, $\alpha = 2.26$ deg, $Re_\infty = 9.0 \times 10^6$.

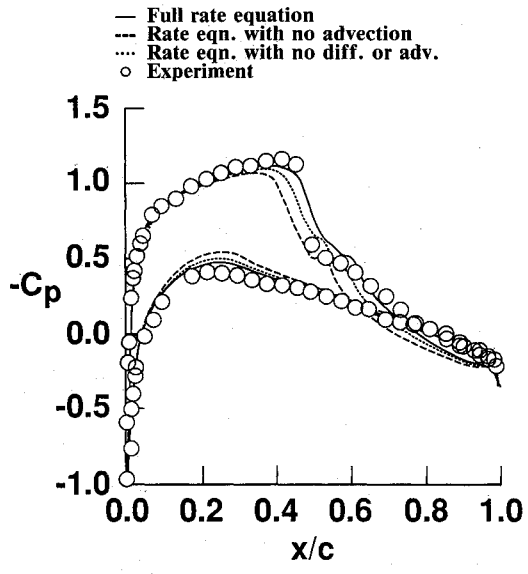

Fig. 13 Comparison of pressure coefficients for the various rate equations vs x/c for the NACA 0012 airfoil at $M_\infty = 0.799$, $\alpha = 2.26$ deg, $Re_\infty = 9.0 \times 10^6$.

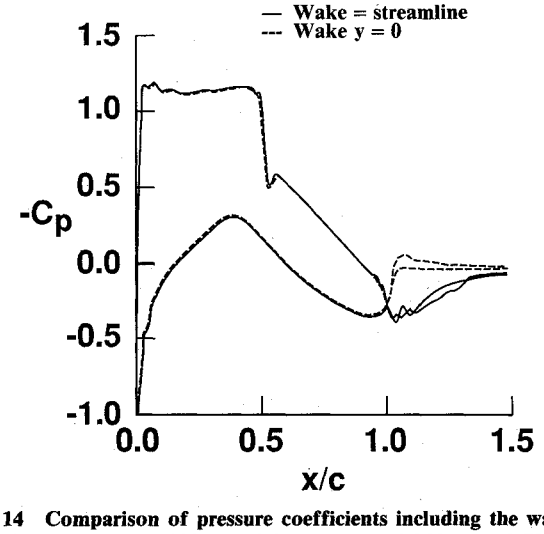

Fig. 14 Comparison of pressure coefficients including the wake vs x/c for the RAE 2822 airfoil at $M_\infty = 0.730$, $\alpha = 2.78$ deg, $Re_\infty = 6.5 \times 10^6$.

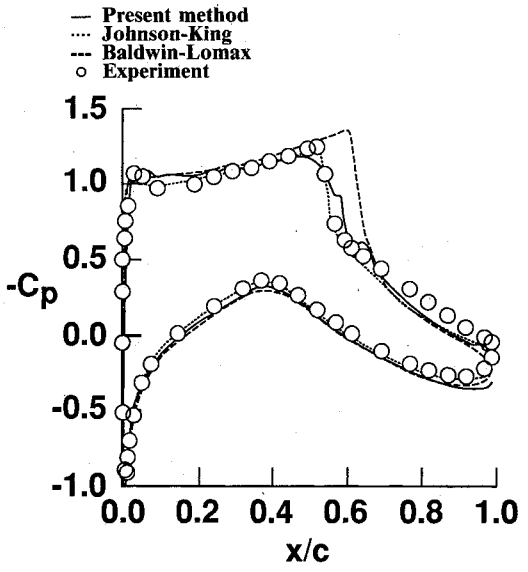

Fig. 15 Comparison of pressure coefficients for different solution methods vs x/c for the RAE 2822 airfoil at $M_\infty = 0.750$, $\alpha = 2.81$ deg, $Re_\infty = 6.2 \times 10^6$.

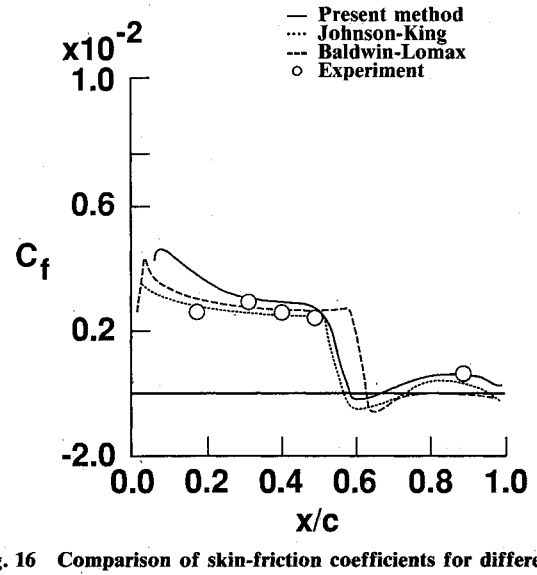

Fig. 16 Comparison of skin-friction coefficients for different solution methods vs x/c for the RAE 2822 airfoil at $M_\infty = 0.750$, $\alpha = 2.81$ deg, $Re_\infty = 6.2 \times 10^6$.

advection is in line with Townsend's description of turbulent shear layers,[20] in which he explained that a useful approximation could be obtained by examining only the turbulent energy production and dissipation. However, the discrepancy between the full rate equation results and the results using the rate equation without diffusion or normal advection was small only for the attached flow case, indicating that Townsend's argument is not valid for separated flow.

Many researchers who use body-fitted grids for this type of viscous-inviscid interaction find it convenient to take the wake cut as the grid line emanating from the trailing edge. This often corresponds to the wake being positioned at $y = 0$ rather than the more realistic location of the wake streamline. The treatment presented here is based on an approximate method for locating the wake cut. When this method is compared to setting the wake at $y = 0$, more realistic results were obtained. Figure 14 shows the pressure coefficient over the RAE 2822 airfoil and wake at $M_\infty = 0.73$, $\alpha = 2.78$ deg, and $Re_\infty = 6.5 \times 10^6$. When the wake is chosen as the streamline from the trailing edge, a more gradual change in the pressure distribution is indicated throughout the wake region.

The present method was compared with two Navier–Stokes solutions reported by Coakley[19] for the RAE 2822 airfoil at $M_\infty = 0.75$, $\alpha = 2.81$ deg, and $Re_\infty = 6.2 \times 10^6$. Figures 15 and 16 show the pressure and skin-friction distributions, respectively, for the nonequilibrium, full rate equation case compared with experimental data and the Baldwin–Lomax and Johnson–King turbulence models. The results show good agreement between the present method and the Navier–Stokes solutions employing the Johnson and King model. This is to be expected because the rate equation employed here and that used in the Johnson and King model were derived from the turbulent kinetic energy equation and contained similar terms.

Concluding Remarks

A time-dependent viscous-inviscid interaction algorithm using Cartesian grids has been developed and used to study transonic turbulent flows past airfoils. Both equilibrium and nonequilibrium effects are considered. Moreover, a procedure is developed that calculates the wake cut as part of the solution.

The calculations illustrate the influence of diffusion and normal advection on shock location and the importance of keeping both terms in the rate equation. In spite of the fact that an eddy-viscosity turbulence model is used in evaluating the dissipation integral, relatively good agreement with experiments is indicated. Further improvements can be obtained by incorporating a turbulence model valid for separated flows.

Appendix: Turbulence Correlations

The various shape factors used in this work are as follows[7,8]:

$$H_{\delta^*} = \bar{H}(1 + 0.113M_e^2) + 0.290M_e^2 \tag{A1}$$

$$H_{\theta^*} = \frac{\bar{H}_{\theta^*} + 0.028M_e^2}{1 + 0.014M_e^2} \tag{A2}$$

$$H_{\delta^{**}} = \left(\frac{0.064}{\bar{H} - 0.8} + 0.251\right)M_e^2 \tag{A3}$$

$$\frac{\theta}{\bar{\theta}} = 1 - \frac{0.92M_e^2}{7.09 + M_e^2}\tanh[1.49(\bar{H} - 0.9)] \tag{A4}$$

where $\bar{H}_{\theta^*}$ is represented by

$$\bar{H}_{\theta^*} = \frac{1}{9}\left(\bar{H} + 7 + \frac{10}{\bar{H}}\right), \quad \bar{H} \le 5$$

$$= \frac{1}{18}\left(\bar{H} + 24 - \frac{5}{\bar{H}}\right), \quad \bar{H} > 5 \tag{A5}$$

The correlation for skin friction is

$$c_f = \frac{\dfrac{0.3e^{-1.33\bar{H}}}{(\log_{10}\overline{Re_\theta})^{1.74 + 0.31\bar{H}}}(1.1 \times 10^{-4})\left[\tanh\left(4 - \dfrac{\bar{H}}{0.875}\right) - 1\right]}{\left(1 + \dfrac{\gamma - 1}{2}M_e^2\right)^{1/2}} \tag{A6}$$

Acknowledgments

This work was supported in part by NASA Grant NGT 34-002-801, and the Hypersonic Aerodynamics Program Grant NAGW-1072 funded jointly by NASA, Air Force Office of Scientific Research, and Office of Naval Research. The authors would like to acknowledge many helpful discussions with Dr. James L. Thomas of NASA Langley Research Center.

References

[1]Clark, D. K., Salas, M. D., and Hassan, H. A., "Euler Calculations for Multi-Element Airfoils Using Cartesian Grids," *AIAA Journal*, Vol. 24, March 1986, pp. 353–356.

[2]Gaffney, R. L., Hassan, H. A., and Salas, M. D., "Euler Calculations for Wings Using Cartesian Grids," AIAA Paper 87-0356, Jan. 1987.

[3]Frymier, P. D., Jr., Salas, M. D., and Hassan, H. A., "Navier-Stokes Calculations Using Cartesian Grids, I. Laminar Flows," *AIAA Journal*, Vol. 20, Oct. 1988, pp. 1181–1188.

[4]Swafford, T. W. and Whitfield, D. L., "Time-Dependent Solution of Three-Dimensional Compressible Turbulent Integral Boundary-Layer Equations," *AIAA Journal*, Vol. 23, July 1985.

[5]Donegan, T., "Unsteady Viscous-Inviscid Interaction Procedures for Transonic Airfoil Flows," M.S. Thesis, Univ. of Tennessee, TN, Dec. 1983.

[6]Whitfield, D. L., Swafford, T. W., and Jacocks, J. L., "Calculation of Turbulent Boundary Layers with Separation and Viscous-Inviscid Interactions," *AIAA Journal*, Vol. 19, Oct. 1981, pp. 1315–1322.

[7]Thomas, J. L., "Transonic Viscous-Inviscid Interaction Using Euler and Inverse Boundary-Layer Equations," Ph.D. Dissertation, Mississippi State Univ., Mississippi State, MS, Dec. 1983.

[8]Thomas, J. L., "Integral Boundary-Layer Models for Turbulent Separated Flows," AIAA Paper 84-1615, June 1984.

[9]Green, J. E., Weeks, D. M., and Brooman, J. W. F., "Prediction of Turbulent Boundary Layers and Wakes in Incompressible Flow by a Lag Entrainment Method," Royal Aircraft Establishment, Rept. and Memo. No.T 3791, Jan. 1973.

[10]Johnson, D. A. and King, L. S., "A New Turbulent Closure Model for Boundary-Layer Flows with Strong Adverse Pressure Gradients and Separation," AIAA Paper 84-0175, Jan. 1984.

[11]Le Balleur, J. C., "Numerical Flow Calculations and Viscous-Inviscid Interaction Techniques," *Computational Methods in Viscous Flow*, Vol. 3, edited by W. G. Habashi, Pineridge Press, Swansea, England, 1984, pp. 419–450.

[12]Carter, J. E., "A New Boundary-Layer Inviscid Interaction Technique for Separated Flow," AIAA Paper 79-1450, July 1979.

[13]Clauser, F. H., "Turbulent Boundary Layers in Adverse Pressure Gradients," *Journal of Aeronautical Sciences*, Vol. 21, Feb. 1954, pp. 91–108.

[14]Bradshaw, P., Ferris, D. H., and Atwell, N. P., "Calculation of Boundary-Layer Development Using the Turbulent Energy Equation," *Journal of Fluid Mechanics*, Vol. 28, Pt. 3, May 1967, pp. 593–616.

[15]Lighthill, M. J., "On Displacement Thickness," *Journal of Fluid Mechanics*, Vol. 4, Pt. 4, Aug. 1958, pp. 383–392.

[16]Jameson, A., Schmidt, W., and Turkel, E., "Numerical Solutions of the Euler Equations by Finite-Volume Methods Using Runge-Kutta Time-Stepping Schemes," AIAA Paper 81-1259, June 1981.

[17]Cook, P. H., McDonald, M. A., and Firmin, M. C. P., "Aerofoil RAE 2822-Pressure Distributions and Boundary Layer and Wake Measurements," AGARD Rept. AR-138, Experimental Data Base for Computer Program Assessment, May 1979.

[18]Harris, C. D., "Two-Dimensional Aerodynamic Characteristics of the NACA 0012 Airfoil in the Langley 8-foot Transonic Pressure Tunnel," NACA TM-81927, April 1981.

[19]Coakley, T. J., "Numerical Simulation of Viscous Transonic Airfoil Flows," AIAA Paper 87-0416, Jan. 1987.

[20]Townsend, A. A., *The Structure of Turbulent Shear Flow*, Cambridge University Press, London, 1956, Chap. 7.